Polarized photons from the early stages of relativistic heavy-ion collisions

Sigtryggur Hauksson[*]
Institut de Physique Théorique, CEA/Saclay, Université Paris-Saclay, 91191, Gif sur Yvette, France

Charles Gale[†]
Department of Physics, McGill University, 3600 University Street, Montréal, Québec, Canada H3A 2T8

(Received 13 July 2023; accepted 6 February 2024; published 4 March 2024)

The polarization of real photons emitted from early-time heavy-ion collisions is calculated, concentrating on the contribution from bremsstrahlung and quark-antiquark annihilation processes at leading order in the strong coupling. The effect of an initial momentum space anisotropy of the parton distribution is evaluated using a model for the nonequilibrium scattering kernel for momentum broadening. The effect on the photon polarization is reported for different degrees of anisotropy. The real photons emitted early during in-medium interactions will be dominantly polarized along the beam axis.

DOI: 10.1103/PhysRevC.109.034902

I. INTRODUCTION

The theory of the nuclear strong interaction, quantum chromodynamics (QCD), features a transition from a phase where the relevant degrees of freedom are quarks and gluons—at high temperature—to one where the appropriate basis consists of composite hadrons at a lower temperature. This transition has been predicted by several theoretical approaches, including the nonperturbative field-theoretical framework of lattice QCD [1]. Decades of intense theoretical effort have revealed that the transition from confined hadrons to partons is not a thermodynamic phase transition in the proper sense but rather an analytic crossover [2]. On the experimental side, this exotic state of strongly interacting matter—the quark-gluon plasma (QGP)—has been observed in the relativistic collisions of nuclei ("heavy-ions") performed at the BNL Relativistic Heavy-Ion Collider (RHIC), and its existence has been later confirmed by experiments performed at the CERN Large Hadron Collider (LHC) [3]. There also is strong evidence supporting the presence of QGP in smaller systems [4].

The theoretical tools developed to study the dynamics of nuclear collisions and the formation of the QGP typically consist of multistage models, rendered necessary by the complexity of the nuclear reaction [5–9]. As this multistage modeling of relativistic heavy-ion collisions covers a variety of dynamical conditions ranging from far from equilibrium initial states to almost ideal fluid dynamics, it is important to critically examine its different eras. In searching for observables capable of revealing the different modeling epochs, penetrating probes such as real and virtual photons impose themselves. Electromagnetic variables are emitted at all stages of the collision and as such can report on local conditions at their creation point [10]. The largest uncertainty in the chain of models currently lie at the beginning, in the time span preceding "hydrodynamization". Early in the history of the collision, photon emission is liable to occur in media far from equilibrium, and this necessitate a dedicated theoretical treatment [11,12].

This study will consider those photons emitted in the early stages of heavy-ion collisions, and will focus more specifically on their polarization state as a probe of the medium at early times. As our calculation only relies on the medium having a pressure anisotropy, or equivalently a momentum anisotropy in parton distribution, it holds both before hydrodynamization as well as in the beginning of the hydrodynamic stage while pressure anisotropy still persists. Some previous estimates for photon polarization at early times considered leading order direct photon production channels like those of the Compton process and $q\bar{q}$ annihilation [13–15]. It is known that an equally important contribution as those two—at the same order in α_s, the strong coupling constant—is that associated with the Landau-Pomeranchuk-Migdal effect (LPM) [16–18]. That contribution, evaluated for a medium out of equilibrium forms the basis of this work. It is fair to remind readers that the measurement of real photon polarization states is challenging, owing to the complications related to the external conversions into lepton pairs in experimental detectors. The angular distribution of this pairs will reflect the polarization state. A more realistic proposition is a measurement of virtual photon polarization states, as measured through an internal conversion process leading to a dilepton final state. Consequently, the goal of our work is to first set the foundations for subsequent such evaluations and to perform a first estimate of the polarization signature of an early, nonequilibrium, strongly interacting medium.

Our paper is organized as follows. Section II lays out the building blocks of our nonequilibrium formalism. The section following that one discusses the collision kernel used to

[*]sigtryggur.hauksson@ipht.fr
[†]gale@physics.mcgill.ca

 ©2024 American Physical Society

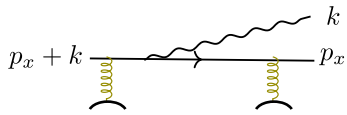

FIG. 1. Photon radiation through medium-induced bremsstrahlung off a quark.

model the medium interactions. The numerical methods used to obtain the production rate of polarized photons are discussed in Sec. IV. Results and conclusion constitute Secs. V and VI, respectively. We present analytical and numerical details in the Appendices.

II. POLARIZED PHOTON EMISSION

The quark-gluon plasma radiates photons through two different processes at leading order in perturbation theory. (See [19] for higher order corrections.) These processes are two-to-two scattering with a photon in the final state [20,21], and bremsstrahlung and pair annihilation with a resulting photon [16,18]. Two-to-two scattering on one hand and bremsstrahlung and pair annihilation on the other hand give roughly equal contribution to photon yield in the plasma [17]. While photons from two-to-two scattering have been studied extensively in an anisotropic medium and have been shown to be polarized [13], bremsstrahlung and pair annihilation photons have been studied much less in an anisotropic plasma due to the more complicated physics involved. We consider this now. Polarized photon emission has also been studied in other contexts, including in holography where a background magnetic field is included [22–24], due to vortical flow in the plasma [25], and due to the chiral magnetic effect [26,27]. Dilepton polarization has furthermore been considered in [28–30].

In bremsstrahlung an on-shell photon is emitted collinearly off a quark or an antiquark, see Fig. 1. In vacuum this process would be kinematically forbidden as an on-shell quark cannot emit an on-shell photon. However, in a medium the process is made possible due to soft gluon kicks from the medium that bring the quark slightly off-shell. These kicks have momentum $\sim g\Lambda$, where Λ is a hard scale akin to temperature and g is the coupling constant. The off-shellness of the quark is therefore of order $P^2 \sim g^2\Lambda^2$ meaning that the emission takes time $t \sim p/P^2 \sim 1/g^2\Lambda$, where p is the quark momentum. During this time the quark can receive arbitrarily many soft gluon kicks. While each of these kicks only takes time $1/g\Lambda$, the mean-free time between two such kicks is of order $1/g^2\Lambda$ which is comparable to the emission time of the photon. Any

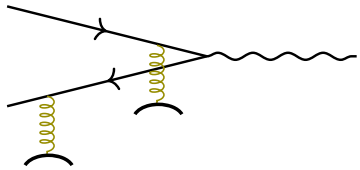

FIG. 2. Photon radiation through medium-induced quark-antiquark pair annihilation.

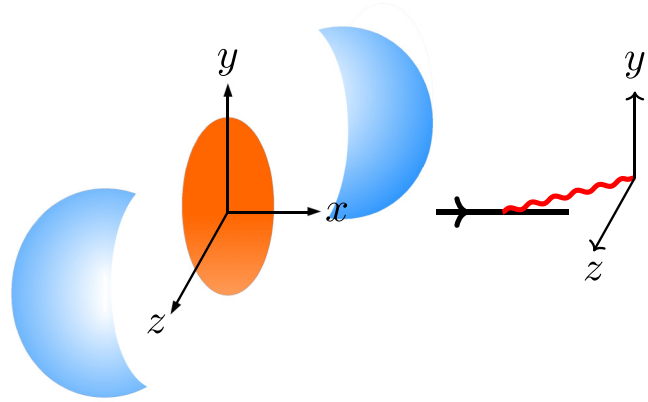

FIG. 3. Our choice of coordinate system. The z axis is chosen to be along the beam axis. For a photon emitted at midrapidity we choose the x axis to be along its momentum. The photon (in red) can either be transversely polarized along the beam axis (z axis) or transversely polarized orthogonal to the beam axis, i.e., along the y axis.

number of kicks can thus be imparted on the quark during the emission of the photon, meaning that at leading order in perturbation theory one needs a dressed vertex that resums arbitrarily many soft gluon kicks [16,18,31]. In an analogous fashion a quark-antiquark pair can annihilate and radiate a photon due to medium kicks, see Fig. 2.

Calculating the polarized rate of photon emission through bremsstrahlung and pair annihilation requires extending the framework developed in [11,16,18] for unpolarized photon emission. To fix ideas we choose the coordinate system in Fig. 3. The z axis lies along the beam axis in a heavy-ion collision. We consider a photon at midrapidity and orient the coordinate system so that the x axis lies along its momentum $\mathbf{k}$. The momentum of the photon can of course have any direction in the plane transverse to the beam axis; aligning it with the short axis of the plasma as in Fig. 3 is simply for illustration.[1] As an on-shell photon is transversely polarized, the polarization basis can be chosen as $\epsilon_z = (0, 0, 0, 1)$ and $\epsilon_y = (0, 0, 1, 0)$. The photon is thus polarized along the beam axis or transverse to the beam axis.

The derivation of polarized photon emission is similar to that for unpolarized emission found in [11,16,18]. In both cases one evaluates the diagram in Fig. 4 which includes arbitrarily many soft gluon kicks. These soft kicks do not have enough energy to flip the helicity of quarks and therefore their resummation is done in the same way for polarized and unpolarized photon emission. This resummation happens on the level of the three-point function in Fig. 5 which we call $\mathbf{f} = (f_z, f_y)$, see [16,18] for further details. It solves the

[1]In this work, the net polarization of photons emitted from a fluid cell is independent of the angular orientation in the transverse plane as we focus on the effect of longitudinal expansion. This could be generalized to include transverse expansion which breaks this symmetry. Our formalism could also easily be extended to photons at finite rapidity.

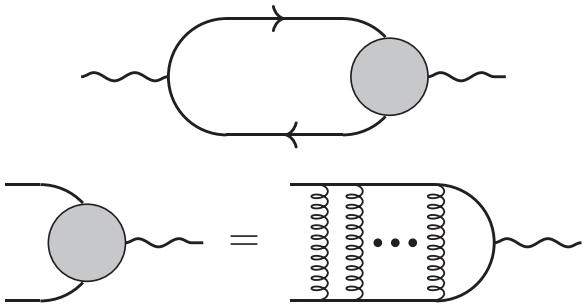

FIG. 4. Diagram for medium-induced photon emission. The gluon rungs are responsible for momentum broadening.

integrodifferential equation

$$2\mathbf{p}_\perp = i\delta E\mathbf{f}(\mathbf{p}_\perp) + \int \frac{d^2q_\perp}{(2\pi)^2}\,\mathcal{C}(\mathbf{q}_\perp)[\mathbf{f}(\mathbf{p}_\perp) - \mathbf{f}(\mathbf{p}_\perp + \mathbf{q}_\perp)], \tag{1}$$

where

$$\delta E = \frac{k}{2p(p+k)}[p_\perp^2 + m_\infty^2]. \tag{2}$$

The central ingredient in this equation is the collision kernel $\mathcal{C}(\mathbf{q}_\perp)$ which is defined as

$$\mathcal{C}(\mathbf{q}_\perp) = g^2 C_F \int \frac{dq^0 dq_x}{(2\pi)^2}\, D_{rr}^{\mu\nu}(Q) v_\mu v_\nu\, 2\pi\delta(v\cdot Q), \tag{3}$$

where $v^\mu = (1,1,0,0)$ is the four-velocity of the quark emitting a photon and $D_{rr}^{\mu\nu}(Q)$ is the statistical propagator for gluons in the medium. The collision kernel gives the rate for a quark to receive soft gluon kicks of transverse momentum $\mathbf{q}_\perp$. It gives rise to a gain term and a loss term in Eq. (1). This equation furthermore has a source term $2\mathbf{p}_\perp$ which denotes the transverse momentum at the hard emission vertex.

We have shown that the effect of soft gluon kicks on photon emission is described by Eq. (1) which takes the same form for polarized or unpolarized emission. On the contrary, the hard emission vertices must be treated differently for polarized emission. We first consider a bare quark loop stripped of soft gluon kicks, see Fig. 6. Here, the spinor trace for hard emission vertices with a z-polarized photon takes the form

$$H^{zz} := \epsilon_\mu^z \epsilon_\nu^{z*} \mathrm{Tr}\,[\gamma^\mu(\not{K} + \not{P})\gamma^\nu \not{P}], \tag{4}$$

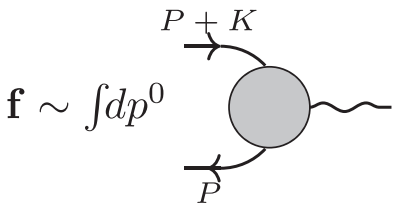

FIG. 5. Definition of $\mathbf{f}$ in terms of the resummed three-point vertex. See [16,18] for further details.

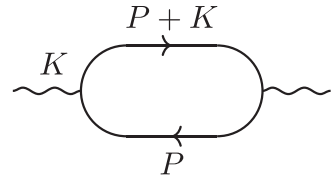

FIG. 6. Definition of momenta in photon emission.

where ϵ_μ^z is the photon polarization tensor for z polarization. This trace is most easily evaluated by using that, e.g.,

$$\not{P} = \sum_s u^s(\mathbf{p})\bar{u}^s(\mathbf{p}), \tag{5}$$

where the sum is over spin states and

$$u^s(\mathbf{p}) = \sqrt{2p}\begin{bmatrix} \frac{1-\sigma\cdot\hat{\mathbf{p}}}{2}\xi^s \\ \frac{1+\sigma\cdot\hat{\mathbf{p}}}{2}\xi^s \end{bmatrix} \tag{6}$$

are helicity states of quarks [32]. Here, ξ^s form a basis for two-component spin states. An explicit calculation shows that

$$\begin{aligned} H^{zz} &= \sum_{s,t}[\gamma^z u^s(\mathbf{p}+\mathbf{k})\bar{u}^s(\mathbf{p}+\mathbf{k})\gamma^z u^t(\mathbf{p})\bar{u}^t(\mathbf{p})] \\ &= \frac{8p^x(p^x+k)}{(p^x)^2(p^x+k)^2}\big[(2p^x+k)^2 p_{\perp z}^2 + k^2 p_{\perp y}^2\big]. \end{aligned} \tag{7}$$

Similarly, the spinor trace for emission of y-polarized photons is

$$H^{yy} = \frac{8p^x(p^x+k)}{(p^x)^2(p^x+k)^2}\big[(2p^x+k)^2 p_{\perp y}^2 + k^2 p_{\perp z}^2\big]. \tag{8}$$

This is the same as Eq. (7), except that $p_{\perp z}^2$ and $p_{\perp y}^2$ have been interchanged.

An explicit calculation of the diagram in Fig. 6 then shows that it gives rate[2]

$$\begin{aligned} k\frac{d\Gamma_z}{d^3\mathbf{k}} = \frac{6\alpha_{EM}\sum_s q_s^2}{(2\pi)^2}\frac{1}{8}\mathrm{Re}\int \frac{d^4P}{(2\pi)^4}\, F(\mathbf{k}+\mathbf{p})[1-F(\mathbf{p})]H_{zz} \\ \times \frac{1}{2E_\mathbf{p}}\frac{1}{p^0 - E_\mathbf{p} + i\epsilon}\,\frac{1}{2E_{\mathbf{k}+\mathbf{p}}}\frac{1}{p^0 + k^0 - E_{\mathbf{k}+\mathbf{p}} - i\epsilon}. \end{aligned} \tag{9}$$

The last line in this expression has the propagator for the two quarks with momenta P and $P+K$. This expression furthermore includes the spinor trace H_{zz} and momentum factors[3]

$$F(p^x) = \theta(p^x)n_f(\mathbf{p}) + \theta(-p^x)(1 - n_f(-\mathbf{p})). \tag{10}$$

[2]As we take the real part of a purely imaginary number this diagram evaluates to zero as expected for the rate of on-shell quarks emitting an on-shell photon with no medium kicks. Our purpose here is simply to explain the structure of such calculations before going to the full case that includes medium kicks.

[3]We have assumed that there is no chiral imbalance in the medium and that the baryon chemical potential vanishes, so that quarks and antiquarks of both helicities have the same momentum distribution n_f.

The momentum factor in Eq. (10) can be easily understood. Bremsstrahlung off a quark corresponds to $p^x > 0$ as then the momentum factor is

$$F(k^x + p^x)[1 - F(p^x)] = n_f(k^x + p^x)(1 - n_f(p^x)) \quad (11)$$

which describes a quark with momentum $k^x + p^x$ that emits a photon with momentum k^x and thus has momentum p^x left in the final state. Similarly, $p^x < -k$ corresponds to bremsstrahlung off an antiquark. Furthermore, $-k < p_x < 0$ corresponds to quark-antiquark pair annihilation with momentum factor

$$F(k^x + p^x)[1 - F(p^x)] = n_f(k^x + p^x)n_f(-p^x), \quad (12)$$

where both the quark and the antiquark are in the initial state.

Continuing with our evaluation of Fig. 6, we do the p^0 integral in Eq. (9) with contour integration. A rewriting using that $\delta E = E_{\mathbf{p}} + k^0 - E_{\mathbf{p}+\mathbf{k}}$ at leading order, then shows that

$$k\frac{d\Gamma_z}{d^3\mathbf{k}} = \frac{6\alpha_{EM}\sum_s q_s^2}{(2\pi)^3}\int_{-\infty}^{\infty} dp^z\, F(\mathbf{k}+\mathbf{p})[1 - F(\mathbf{p})] \times \frac{1}{2}\frac{1}{4(p^x)^2(p^x+k)^2}\left[(2p^x + k)^2 A_z^0 + k^2 A_y^0\right]. \quad (13)$$

Here,

$$A_z^0 = \mathrm{Re}\int \frac{d^2p_\perp}{(2\pi)^2} 2p_z f_z^0, \quad (14)$$

where $f_z^0 = 2p_z/i\delta E$ is the solution of Eq. (1) without any soft gluon kicks, and similarly for A_y^0.

A full calculation of the rate of polarized photon emission requires evaluating the diagram in Fig. 4. This is obtained in the same way as the bare quark loop in Fig. 6, except that one replaces the bare vertex by a resummed vertex $\mathbf{f}(\mathbf{p}_\perp)$ which includes gluons rungs and obeys the integral equation in Eq. (1). This means that in Eq. (13) one replaces A_0^z and A_0^y by

$$A_z = \mathrm{Re}\int \frac{d^2\mathbf{p}_\perp}{(2\pi)^2}\, 2p_z f_z(\mathbf{p}_\perp),$$
$$A_y = \mathrm{Re}\int \frac{d^2\mathbf{p}_\perp}{(2\pi)^2}\, 2p_y f_y(\mathbf{p}_\perp), \quad (15)$$

where $\mathbf{f}$ solves the full integrodifferential equation in Eq. (1). Thus the total rate for polarized photon production through bremsstrahlung and pair annihilation can be written as

$$k\frac{d\Gamma_z}{d^3\mathbf{k}} = \frac{6\alpha_{EM}\sum_s q_s^2}{(2\pi)^3}\int_{-\infty}^{\infty} dp^z\, F(\mathbf{k}+\mathbf{p})[1 - F(\mathbf{p})] \times\frac{1}{2}\frac{1}{4(p^x)^2(p^x+k)^2}\left[(2p^x + k)^2 A_z + k^2 A_y\right] \quad (16)$$

and

$$k\frac{d\Gamma_y}{d^3\mathbf{k}} = \frac{6\alpha_{EM}\sum_s q_s^2}{(2\pi)^3}\int_{-\infty}^{\infty} dp^z\, F(\mathbf{k}+\mathbf{p})[1 - F(\mathbf{p})] \times \frac{1}{2}\frac{1}{4(p^x)^2(p^x+k)^2}[k^2 A_z + (2p^x + k)^2 A_y]. \quad (17)$$

We can now easily see that in an anisotropic medium, these processes give polarized photon emission. In an isotropic medium, the collision kernel in Eq. (3) is by definition isotropic, $\mathcal{C}(\mathbf{q}_\perp) = \mathcal{C}(q_\perp)$ and one can show that Eq. (1) is solved by $\mathbf{f} = \mathbf{p}_\perp \hat{f}(p_\perp)$ for some function $\hat{f}$. Then $A_z = A_y$ and one gets the same rate of emitting z-polarized and y-polarized photons from Eqs. (16) and (17). In an anisotropic medium, $\mathcal{C}(\mathbf{q}_\perp)$ depends not only on the magnitude of the kick $q_\perp$ but also on its orientation. In other words, when writing

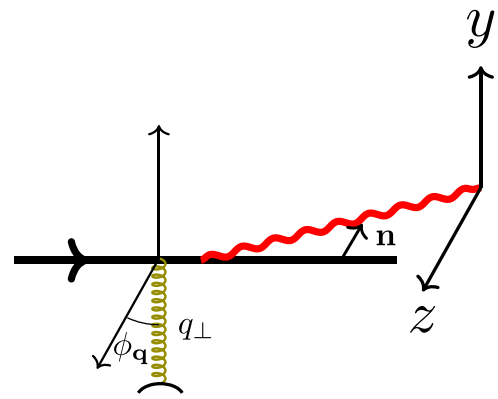

FIG. 7. Definition of the quantities $\mathbf{n}$ (the vector between the outgoing quark and photon) and $\phi_{\mathbf{q}}$ (the angle defining a soft gluon kick of magnitude $q_\perp$). The photon can be polarized in the y or the z directions which are transverse to its direction of motion, see also Fig. 3.

$$\mathbf{q}_\perp = (q_z, q_y) = q_\perp(\cos\phi_{\mathbf{q}}, \sin\phi_{\mathbf{q}}) \quad (18)$$

the collision kernel depends on both $\phi_{\mathbf{q}}$ and $q_\perp$, see Fig. 7. This leads to $\mathbf{f}$ having more complicated angular dependence so that $A_z \neq A_y$. Therefore, photon emission from an anisotropic medium is polarized with $d\Gamma_z \neq d\Gamma_y$.

To understand Eqs. (16) and (17) better, it is helpful to focus on the case of bremsstrahlung off a quark. The rate of producing a z-polarized photons with momentum k through that process is

$$k\frac{d\Gamma_z}{d^3\mathbf{k}} = \frac{6\alpha_{EM}\sum_s q_s^2}{(2\pi)^3}\, 2\int_0^{\infty} dp_x\, \frac{k}{8p_x^2(k+p_x)} \times n_f(k+p_x)[1 - n_f(p_x)](F_{\mathrm{in}}(\zeta)A_z + F_{\mathrm{out}}(\zeta)A_y), \quad (19)$$

where momenta are defined in Fig. 1 and $\zeta = k/(p_x + k)$ is the momentum fraction of the photon. Similarly, the rate of producing y-polarized photons is

$$k\frac{d\Gamma_y}{d^3\mathbf{k}} = \frac{6\alpha_{EM}\sum_s q_s^2}{(2\pi)^3}\, 2\int_0^{\infty} dp_x\, \frac{k}{8p_x^2(k+p_x)} \times n_f(k+p_x)[1 - n_f(p_x)](F_{\mathrm{in}}(\zeta)A_y + F_{\mathrm{out}}(\zeta)A_z), \quad (20)$$

where A_z and A_y have been interchanged relative to Eq. (19). Here,

$$F_{\mathrm{in}}(\zeta) = \frac{(2-\zeta)^2}{\zeta} \quad (21)$$

and

$$F_{\mathrm{out}}(\zeta) = \zeta \quad (22)$$

are exactly the usual polarized splitting functions [33] for photon emission.

Equations (19) and (20) for polarized photon emission can be understood intuitively. We consider a z-polarized photon for concreteness. As the photon travels in the x direction, the splitting plane of the photon and the outgoing quark is spanned by $\widehat{\mathbf{e}}_x$ and a vector orthogonal to $\widehat{\mathbf{e}}_x$ which we call $\widehat{\mathbf{n}}$, see Fig. 7. Equations (19) and (20) show that we can project the vector $\widehat{\mathbf{n}}$ on to the y and the z axes and sum over the contributions. For $\widehat{\mathbf{n}}$ in the z direction, the z-polarized photon is polarized in the splitting plane and the hard splitting function is F_{in}. Momentum broadening is quantified by the z component A_z. On the other hand, for $\widehat{\mathbf{n}}$ in the y direction, the z-polarized photon is polarized out of the splitting plane and the hard splitting function is F_{out}. Momentum broadening is then quantified by A_y.

III. MODEL OF THE COLLISION KERNEL IN AN ANISOTROPIC PLASMA

As previously argued, the collision kernel for soft gluon kicks $\mathcal{C}(\mathbf{q}_\perp)$ is anisotropic in heavy-ion collisions which leads to polarization of photons emitted through bremsstrahlung. The ultimate source of the anisotropy in the kernel is longitudinal expansion of the medium along the beam axis. Such a longitudinal expansion gives pressure anisotropy at early and intermediate times with longitudinal pressure P_L less than transverse pressure P_T. On a microscopic level, this means that quark and gluon quasiparticles have an anisotropic momentum distribution with $\langle p_z^2\rangle < \langle p_x^2\rangle, \langle p_y^2\rangle$. This is captured by the distribution introduced in Ref. [34]:

$$f(\mathbf{p}) = \sqrt{1+\xi}\, f_{\text{iso}}\Big(\sqrt{\mathbf{p}^2 + \xi p_z^2}\Big), \tag{23}$$

where f_{iso} is an isotropic distribution, and $\xi > 0$ quantifies the degree of anisotropy. The prefactor $\sqrt{1+\xi}$ ensures that the number density of quarks and gluons is the same as in equilibrium. A simple calculation gives the pressure anisotropy P_T/P_L in terms of the momentum space anisotropy ξ, linking the macroscopic and microscopic descriptions.[4]

Ideally, one would want to calculate the collision kernel for momentum broadening, $\mathcal{C}(\mathbf{q}_\perp)$, directly from Eq. (23). Such a calculation would use that the hard quasiparticles in Eq. (23) radiate soft gluons which are then responsible for momentum broadening. This would allow to quantify the degree of photon polarization in a nonequilibrium medium from first principles. Unfortunately, going from Eq. (23) to the collision kernel is difficult in practice, partially due to instabilities that can be present in an anisotropic plasma [36].

In this study, we will use a simple model of the collision kernel in a longitudinally expanding medium. We take inspiration from results for the collision kernel in thermal equilibrium at leading order in perturbation theory [37],

$$\mathcal{C}_{\text{eq}}(\mathbf{q}_\perp) = g^2 C_F T\left(\frac{1}{q_\perp^2} - \frac{1}{q_\perp^2 + m_{D0}^2}\right). \tag{24}$$

[4]Specifically, $P_T/P_L = \frac{1}{2}\frac{\sqrt{\xi}+(\xi-1)\arctan\sqrt{\xi}}{\arctan\sqrt{\xi}-\sqrt{\xi}/(1+\xi)}$, see, e.g., [35].

Here, m_{D0}^2 is the equilibrium Debye mass which describes screening of electric fields. (The equilibrium kernel has furthermore been evaluated at next-to-leading order [38], as well as on the lattice, see, e.g., [39,40].) In our anisotropic model, we replace the equilibrium Debye mass by its anisotropic extension[5] found in [34]

$$m_D^2(\phi_{\mathbf{q}}) = \left(1 - \frac{2\xi}{3}\right)m_{D0}^2 + \xi m_{D0}^2 \cos^2\phi_{\mathbf{q}}, \tag{25}$$

so that

$$\mathcal{C}(\mathbf{q}_\perp) = g^2 C_F \Lambda\left(\frac{1}{q_\perp^2} - \frac{1}{q_\perp^2 + m_D^2(\phi_{\mathbf{q}})}\right). \tag{26}$$

The anisotropic correction has an angular dependence with more broadening in the z direction than in the y direction. To simplify calculations, we expand the collision kernel in ξ, writing

$$\mathcal{C}(\mathbf{q}_\perp) \approx g^2 C_F \Lambda\left(\frac{1}{q_\perp^2} - \frac{1}{q_\perp^2 + m_{D0}^2} + \frac{-2\xi m_{D0}^2/3 + \xi m_{D0}^2\cos^2\phi_{\mathbf{q}}}{\left(q_\perp^2 + m_{D0}^2\right)^2}\right), \tag{27}$$

where Λ is a hard scale, akin to temperature.

Equation (27) is a toy model for the collision kernel, intended to illustrate how an anisotropic kernel leads to polarized photon emission and to estimate the magnitude of this effect. This toy model only includes changes to the screening of electric fields in an anisotropic medium and not the myriad other nonequilibrium effects that can arise. Nevertheless, this collision kernel can be motivated by theoretical arguments making us believe that it captures some of the salient features of the full non-equilibrium kernel.

In general the collision kernel is defined by

$$\mathcal{C}(\mathbf{q}_\perp) = g^2 C_F \int \frac{dq^0 dq_x}{(2\pi)^2}\, D_{rr}^{\mu\nu}(Q) v_\mu v_\nu\, 2\pi\delta(v\cdot Q), \tag{28}$$

where $v^\mu = (1,1,0,0)$ is the four-velocity of the quark emitting a photon. The kernel depends on the statistical correlator for gluons in the medium,

$$D_{rr}(Q) := \tfrac{1}{2}\langle\{A,A\}\rangle(Q) = D_{\text{ret}}(Q)\Pi(Q)D_{\text{adv}}(Q) \tag{29}$$

which characterizes the occupation density of a pair of soft gluons. We have omitted Lorentz indices for simplicity. This statistical correlator contains information on how the soft gluons are emitted by hard quasiparticles with rate $\Pi(Q)$ and then propagate in the medium according to the retarded propagator $D_{\text{ret}}(Q) = i/(Q^2 - \Pi_{\text{ret}})$ and the advanced propagator $D_{\text{adv}} = -D_{\text{ret}}^*$.

Making some heuristic assumptions allows one to employ a sum rule in [37] to motivate the toy model for the collision kernel in Eq. (27), starting from the definitions in Eqs. (3) and (29). The goal is to include anisotropic corrections to the

[5]In [34] this quantity is referred to as m_+^2. We have expanded in small ξ in Eq. (27) but this is simply for convenience and not fundamental to the setup we use.

screening of chromoelectric fields, while ignoring anisotropic corrections to the density of gluons and to change in polarization that occurs during propagation. We work strictly at small anisotropy $\xi \ll 1$, including only effects of order $\mathcal{O}(\xi)$.

The first heuristic assumption is to employ the identity $\Pi(Q) = \frac{\Lambda}{q^0} 2\mathrm{Im}\,\Pi_{\mathrm{ret}}$ which is known as the KMS identity and which expresses detailed balance between production and decay of soft gluons. This is not strictly valid in a nonequilibrium medium and amounts to ignoring anisotropic corrections to the density of gluons. Then one can write

$$D_{rr}(Q) := \frac{\Lambda}{q^0}(D_{\mathrm{ret}} - D_{\mathrm{adv}}). \tag{30}$$

At small anisotropy the retarded propagator in Eq. (30) is

$$D^{\mu\nu}_{\mathrm{ret}}(Q) \approx \frac{P^{\mu\nu}_T}{Q^2 - \Pi_T} + \frac{P^{\mu\nu}_L}{Q^2 - \Pi_L}. \tag{31}$$

Here, we have only included anisotropic corrections to the screening as given by Π_T and Π_L, see Appendix A.

Our second heuristic approximation is to focus on the anisotropic correction to Π_L and ignore those in Π_T. Comparing with the equilibrium calculation [37], this amounts to calculating anisotropic corrections to the term $1/(q_\perp^2 + m_{D0}^2)$ in Eq. (24) while leaving the term $1/q_\perp^2$ as is. This means that we include anisotropic corrections to the screening of chromoelectric fields as given by a Debye mass but do not include anisotropic corrections to the screening of chromomagnetic fields.

The reason we use this approximation is that the sum rule we employ does not work for the transverse screening in Π_T. This is because the term $1/(Q^2 - \Pi_T)$ has a pole in the upper half-complex plane of q_0 corresponding to Weibel instabilities [41]. A formal use of the sum rule would lead to a contribution of the form $1/(q_\perp^2 - m^2)$ which is ill-defined at $q_\perp = m$. The solution to this issue is to use a retarded propagator for soft gluons that includes the mechanism by which non-Abelian interaction caps the growth of the unstable soft gluon modes. This is beyond the scope of this project.

Given these two approximations, one can use the sum rule in [37] nearly directly. The longitudinal retarded self-energy at small anisotropy ξ is

$$\Pi_L(Q) = \Pi_L^0(x) + \xi\left[\frac{1}{6}(1 + 3\cos 2\theta_n)\frac{Q^2}{\mathbf{q}^2}m_{D0}^2 + \Pi_L^0(x)\left(\cos 2\theta_n - \frac{x^2}{2}(1 + 3\cos 2\theta_n)\right)\right], \tag{32}$$

where θ_n is the angle between $\mathbf{q}$ and the anisotropy vector $\mathbf{n} = \mathbf{e}_z$ which defines a preferred direction in Eq. (23) [34]. Here,

$$\Pi_L^0(x) = (x^2 - 1)m_{D0}^2\left[\frac{x}{2}\log\frac{x + 1 + i\epsilon}{x - 1 + i\epsilon} - 1\right] \tag{33}$$

is the equilibrium value. We next do a change of variables in Eq. (3) to $x = q_0/q = q_x/\sqrt{q_x^2 + q_\perp^2}$ so that $q_x^2 = x^2 q_\perp^2/(1 - x^2)$ and $q^2 = q_\perp^2/(1 - x^2)$. Then one should substitute $\cos 2\theta_n = 2(q_z/q)^2 - 1 = 2(1 - x^2)\cos^2\phi_{\mathbf{q}} - 1$ to get dependence only on x, $q_\perp$ and $\phi_{\mathbf{q}}$. This gives that the longitudinal contribution to the collision kernel is

$$\frac{\Lambda g^2 C_F}{\pi}\int_0^1 \frac{dx}{x}\frac{\mathrm{Im}\,\widetilde{\Pi}_L(x,\phi_{\mathbf{q}})}{(\mathbf{q}_\perp^2 + \mathrm{Re}\,\widetilde{\Pi}_L(x,\phi_{\mathbf{q}}))^2 + (\mathrm{Im}\,\widetilde{\Pi}_L(x,\phi_{\mathbf{q}}))^2}, \tag{34}$$

where

$$\widetilde{\Pi}_L(x,\phi_{\mathbf{q}}) = \Pi_L^0(x) + \xi\left[\frac{1}{6}(1 + 3\cos 2\theta_n)(x^2 - 1)m_{D0}^2 + \Pi_L^0(x)\left(\cos 2\theta_n - \frac{x^2}{2}(1 + 3\cos 2\theta_n)\right)\right] \times |_{\cos 2\theta_n = 2(1-x^2)\cos^2\phi_{\mathbf{q}} - 1} \tag{35}$$

has no explicit dependence on $q_\perp$.

An argument nearly identical[6] to the one in [37] then shows that Eq. (34) is

$$g^2 C_F \Lambda\left[\frac{1}{q_\perp^2 + \lim_{x\to\infty}\widetilde{\Pi}_L(x,\phi)} - \frac{1}{q_\perp^2 + \widetilde{\Pi}_L(0,\phi)}\right] = -g^2 C_F \Lambda \frac{1}{q_\perp^2 + m_D^2(\phi_{\mathbf{q}})} \tag{36}$$

since $\widetilde{\Pi}_L(0,\phi) = m_D^2(\phi_{\mathbf{q}})$. Our conclusion is therefore that given our heuristic approximations, the collision kernel is given by Eq. (27). We emphasize that this collision kernel is not intended to capture all of the nonequilibrium physics but to focus on anisotropic corrections to the screening of chromoelectric fields.

IV. NUMERICAL METHOD

We wish to evaluate the rate of polarized photon emission in an anisotropic medium such as that found in a longitudinally expanding quark-gluon plasma. The starting point is Eqs. (19) and (20) which require solving the integrodifferential equation in Eq. (1) numerically, assuming the model for the collision kernel given in Eq. (27). To solve Eq. (1) we go to impact parameter space, i.e., the space Fourier conjugate to $\mathbf{p}_\perp$. Defining

$$\mathbf{f}(\mathbf{b}) = \int \frac{d^2 p_\perp}{(2\pi)^2}\, e^{i\mathbf{p}_\perp\cdot\mathbf{b}}\,\mathbf{f}(\mathbf{p}_\perp), \tag{37}$$

the equation we wish to solve becomes

$$-2i\nabla_b\delta^{(2)}(\mathbf{b}) = \frac{ik}{2p(p+k)}\big[-\nabla_b^2 + m_\infty^2\big]\mathbf{f}(\mathbf{b}) + \mathcal{C}(\mathbf{b})\mathbf{f}(\mathbf{b}), \tag{38}$$

[6]The retarded propagator $1/[x^2 q_\perp^2 - q_\perp^2 - (1 - x^2)\Pi_L(x,\phi)]$ in Eq. 7 in [37] has an extra pole in the upper half-complex plane in the anisotropic case. This pole can be seen by taking the limit $x = k_0/k \to \infty$ in which case the propagator becomes $\sim 1/(1 - x^2)/(q_\perp^2 + (\frac{1}{3} - \frac{1}{3}\xi\cos^2\phi)m_{D0}^2 + \frac{\xi}{3}x^2\cos^2\phi\, m_{D0}^2)$ which has a pole which is parametrically of the form $x \sim \pm i q_\perp/m_D\sqrt{\xi}$ and thus far from the real axis when $\xi \ll 1$. This is not in contradiction with the usual properties of the retarded propagator as we have imposed $q_0 = q_x$ and then search for poles in q_0. One can then show that the correction due to this pole to the sum rule in Eq. 9 in [37] is $\mathcal{O}(\xi^{3/2})$ which is subleading to the $\mathcal{O}(\xi)$ contributions we consider.

where

$$\mathcal{C}(\mathbf{b}) = \int \frac{d^2p_\perp}{(2\pi)^2}\left[1 - e^{i\mathbf{p}_\perp\cdot\mathbf{b}}\right]\mathcal{C}(\mathbf{p}_\perp). \tag{39}$$

A straightforward calculation shows that the collision kernel from Eq. (27) is

$$\mathcal{C}(\mathbf{b}) = \mathcal{C}_0(b) + \xi\,\mathcal{C}_1^{(a)}(b) + \xi\cos 2\beta\,\mathcal{C}_1^{(b)}(b) \tag{40}$$

in impact parameter space, where $\mathbf{b} = (b_z, b_y) = (\cos\beta, \sin\beta)b$. The terms of the collision kernel are given by

$$\mathcal{C}_0(\mathbf{b}) = \frac{g^2C_FT}{2\pi}\left[K_0(m_{D0}b) + \gamma_E + \log\frac{m_{D0}b}{2}\right], \tag{41}$$

$$\mathcal{C}_1^{(a)}(b) = g^2C_FT\frac{1}{8\pi}\frac{M^2}{m_{D0}^2}(m_{D0}bK_1(m_{D0}b) - 1), \tag{42}$$

and

$$\mathcal{C}_1^{(b)}(b) = g^2C_FT\frac{M^2b^2}{4\pi}\left[\frac{2}{(m_{D0}b)^4} - \frac{1}{2m_{D0}b}K_1(m_{D0}b) - \frac{1}{(m_{D0}b)^2}K_2(m_{D0}b)\right]. \tag{43}$$

In order to solve Eq. (38) we do an expansion in small ξ, giving

$$\mathbf{f}(\mathbf{b}) = \mathbf{f}_0(\mathbf{b}) + \xi\mathbf{f}_1(\mathbf{b}) + \cdots. \tag{44}$$

The zeroth order solution in ξ satisfies the usual isotropic equation

$$\frac{ik}{2p(p+k)}\left[-\nabla_b^2 + m_\infty^2\right]\mathbf{f}_0(\mathbf{b}) + \mathcal{C}_0(b)\mathbf{f}_0(\mathbf{b}) = -2i\nabla_b\delta^{(2)}(\mathbf{b}) \tag{45}$$

and can be shown to have angular dependence $\mathbf{f}_0(\mathbf{b}) \sim (\cos\beta, \sin\beta)$. The first order satisfies

$$\frac{ik}{2p(p+k)}\left[-\nabla_b^2 + m_\infty^2\right]\mathbf{f}_1(\mathbf{b}) + \mathcal{C}_0(b)\mathbf{f}_1(\mathbf{b}) = -\left[\mathcal{C}_1^{(a)}(b) + \cos 2\beta\,\mathcal{C}_1^{(b)}(b)\right]\mathbf{f}_0(\mathbf{b}). \tag{46}$$

Due to the angular dependence of the right hand side we can write in full generality

$$f_{1z}(\mathbf{b}) = \cos\beta f_1^{(1z)}(b) + \cos 3\beta\, f_1^{(3)}(b) \tag{47}$$

and

$$f_{1y}(\mathbf{b}) = \sin\beta f_1^{(1y)}(b) + \sin 3\beta\, f_1^{(3)}(b), \tag{48}$$

where these functions solve

$$\mathcal{K}\left[f_1^{(1z)}(\mathbf{b})\right] + \mathcal{C}_0(b)f_1^{(1z)}(\mathbf{b}) = -\left[\mathcal{C}_1^{(a)}(b) + \tfrac{1}{2}\mathcal{C}_1^{(b)}(b)\right]f_0, \tag{49}$$

$$\mathcal{K}\left[f_1^{(1y)}(\mathbf{b})\right] + \mathcal{C}_0(b)f_1^{(1y)}(\mathbf{b}) = -\left[\mathcal{C}_1^{(a)}(b) - \tfrac{1}{2}\mathcal{C}_1^{(b)}(b)\right]f_0 \tag{50}$$

with

$$\mathcal{K}[\mathbf{f}(\mathbf{b})] = -\frac{ik}{2p(p+k)}\left[\frac{d^2}{db^2} + \frac{1}{b}\frac{d}{db} - \frac{1}{b^2} - m_\infty^2\right]\mathbf{f}(\mathbf{b}). \tag{51}$$

(The differential equation for $f_1^{(3)}$ is given in Appendix B.)

Our goal is to evaluate

$$A_z = 2\mathrm{Im}\,\partial_{b_z}f_z(\mathbf{b})\Big|_{b=0} = 2\mathrm{Im}\,\frac{\widehat{\mathbf{b}}\cdot\mathbf{f}_0 + \xi\, f_1^{(1z)}}{b}\Big|_{b=0} \tag{52}$$

and

$$A_y = 2\mathrm{Im}\,\partial_{b_y}f_y(\mathbf{b})\Big|_{b=0} = 2\mathrm{Im}\,\frac{\widehat{\mathbf{b}}\cdot\mathbf{f}_0 + \xi\, f_1^{(1y)}}{b}\Big|_{b=0} \tag{53}$$

which were defined in Eqs. (19) and (20). Thus, we only need to know $f_1^{(1z)}(b)/b$ and $f_1^{(1y)}(b)/b$ in the limit $b \to 0$ where it must be finite. This gives the boundary condition that This is done by demanding that $f_1^{(1z)}$ and $f_1^{(1y)}$ vanish at $b = 0$. The other boundary condition is that the functions vanish as $b \to \infty$ as can be seen from Eq. (37).

To evaluate $f_1^{(1z)}(b)/b$ and $f_1^{(1y)}(b)/b$ at $b = 0$, we demand that the functions $f_1^{(1z)}$ and $f_1^{(1y)}$ vanish at very large b and evolve the functions numerically to small b using Eqs. (49) and (50). In practice, this means that we start the evolution at a large but finite value of b, where $f_1^{(1z)}$ and $f_1^{(1y)}$ are initialized to a small value. A typical numerical solution for f_1^{1z} and f_1^{1y} then blows up as evolved towards $b \to 0$. We must then extract the finite part of our numerical solution. This is done by matching with known, analytic solutions of the differential equations in the small b limit.

For instance, focusing on Eq. (49), we call the particular solution $w(b)$ and the two independent solutions of the homogeneous equation $w_1(b)$ and $w_2(b)$. These are known analytically at small b, see Appendix B. We can write our numerical solution in full generality at small b as

$$f_1^{(1z)}(b) = w(b) + \alpha_1 w_1(b) + \alpha_2 w_2(b), \tag{54}$$

where α_1 and α_2 are found numerically. To extract from this a solution with the right behavior as $b \to 0$, one must in essence subtract a linear combination of w_1 and w_2 which satisfies the boundary condition at $b \to \infty$. Then one is left with a solution which satisfies boundary conditions both at $b = 0$ and $b \to \infty$ and which gives $f_1^{(1z)}(b)/b$ at $b = 0$. This procedure is explained in further detail in Appendix B, see also [37,42,43] for earlier work in the isotropic case. A major difference with the isotropic case is that Eqs. (49) and (50) have a nontrivial right hand side which complicates the matching procedure. For instance, one must find an analytic solution $w(b)$ of the full differential equations at small b, including the right hand side. Furthermore, cancellation errors between solutions of the full differential equation and the homogeneous equation must carefully be avoided to get reliable results, see Appendix B.

V. RESULTS

Figures 8 and 9 are the main results of this work. They show the rate of photon production through bremsstrahlung and pair-annihilation in an anisotropic quark-gluon plasma with fixed anisotropy ξ. The collision kernel is given by Eq. (27) while the momentum distribution of medium quarks

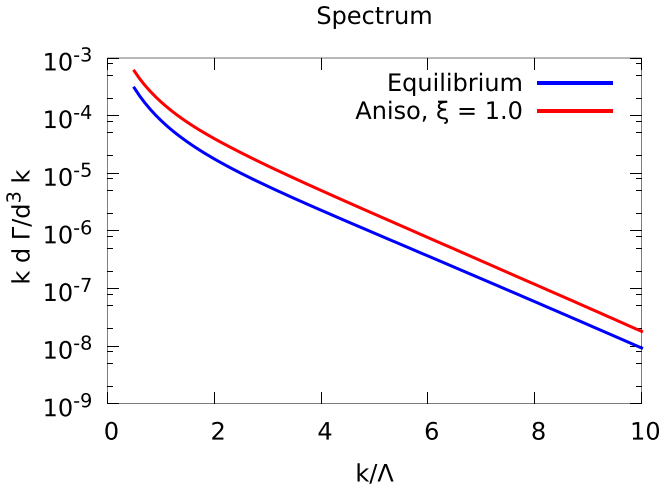

FIG. 8. Spectrum of photons coming from bremsstrahlung and pair annihilation in a plasma at effective temperature Λ. The anisotropic plasma has $\xi = 1.0$.

is

$$f(\mathbf{p}) = \frac{\sqrt{1+\xi}}{e^{\sqrt{p^2+\xi p_z^2}/\Lambda}+1}, \tag{55}$$

where Λ can be seen as an effective temperature. Figure 8 shows the total rate for producing photons at midrapidity and with momentum k, i.e.,

$$k\frac{d\Gamma}{d^3\mathbf{k}} = k\frac{d\Gamma_z}{d^3\mathbf{k}} + k\frac{d\Gamma_y}{d^3\mathbf{k}}, \tag{56}$$

where $k\frac{d\Gamma_z}{d^3\mathbf{k}}$ is the rate of producing photons polarized along the beam axis and $k\frac{d\Gamma_y}{d^3\mathbf{k}}$ is the rate for photons polarized orthogonal to the beam axis and to the photon momentum. Figure 9 shows the degree of polarization at different momenta defined as

$$R = \frac{k\frac{d\Gamma_z}{d^3\mathbf{k}} - k\frac{d\Gamma_y}{d^3\mathbf{k}}}{k\frac{d\Gamma_z}{d^3\mathbf{k}} + k\frac{d\Gamma_y}{d^3\mathbf{k}}}. \tag{57}$$

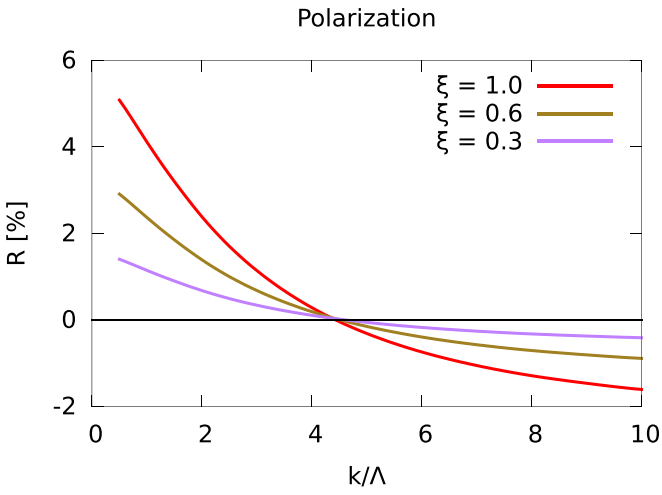

FIG. 9. Degree of polarization of photons emitted from bremsstrahlung and pair annihilation in an anisotropic plasma with $\xi = 1.0$. The quantity R is defined in Eq. (57). We express it in percentages.

These quantities are shown for three values of anisotropy parameter, $\xi = 0.3$, $\xi = 0.6$, and $\xi = 0.9$, which correspond to pressure anisotropy of $P_L/P_T \approx 0.81$, $P_L/P_T \approx 0.68$, and $P_L/P_T \approx 0.57$, respectively. These are rather moderate values of pressure anisotropy which can be found in the early and intermediate stages of heavy-ion collisions.

The spectrum in an anisotropic medium is higher than that in an equilibrium medium at the same effective temperature Λ, as can be seen in Fig. 8. This is due to the factor $\sqrt{1+\xi}$ in the momentum distribution in Eq. (23) which increases the number of quarks with $p_z = 0$ which can emit photons at midrapidity. This effect is partially compensated by anisotropic corrections which reduce the collision kernel $\mathcal{C}(\mathbf{q}_\perp)$ meaning that a given quark receives less momentum broadening, reducing the rate at which it emits photons collinearly.

More interesting is the polarization R as a function of momentum k. As seen in Fig. 9, the polarization has different signs for lower and higher values of the photon energy k: it is along the beam axis for lower values of k while it is orthogonal to the beam axis at higher values of k. This owes to the interplay between bremsstrahlung and pair annihilation. As can be seen from Eqs. (16) and (17), because of the different polarized splitting functions, bremsstrahlung tends to give photons polarized along the z axis, while pair annihilation tends to give polarization along the x axis, see Fig. 3. As bremsstrahlung is suppressed at high k (there are few medium quarks with energy higher than k) x polarization dominates in that regime. On the contrary, pair annihilation is suppressed at low k since the number of quarks with energy less than $k/2$ is phase space suppressed. This gives z-polarized photons in that regime.

Despite the complicated dependence of polarization on photon momentum, polarization along the beam axis dominates and is in principle an observable prediction of our work. This is simply because there are many more photons at lower k and thus their polarization is dominant. Furthermore, in [13] it was shown that photons from two-to-two scattering, which are equally important as bremsstrahlung and pair annihilation photons, are also predominantly polarized along the beam axis, with an even greater magnitude of polarization. Thus a definite and robust prediction of our work is that medium photons are polarized along the beam axis. To go beyond this nevertheless important conclusion and to be able to make a quantitative assessment useful for experiments, more work is needed. First, all photon sources that cannot be subtracted in experiments need to be included, such as prompt photons and photons from the hadronic stage. Second, all photon-producing channels (two-to-two, LPM) have to be included coherently in a calculation that considers an anisotropic medium, and then folded with hydrodynamics or kinetic theory simulations of the medium to get a realistic evolution of the anisotropy and temperature. This requires improving on the calculation of polarized photon production

through two-to-two scattering in [13] by relaxing the assumption of static scatterers and by including HTL resummation in quark mediators. We leave this for future work.

VI. CONCLUSION

In this work, we have calculated for the first time the degree of polarization for photons emitted in bremsstrahlung and off-shell pair annihilation processes in a hot medium consisting of quarks and gluons. Our evaluation includes the LPM regime and is at complete leading order in the strong coupling. The polarization of the real photons originating from bremsstrahlung and annihilation processes depends on the anisotropy of the original parton distribution, and therefore the polarization can instruct us on the dynamics in an environment that is not accessible to the vast majority of probes and observables measured in relativistic heavy-ion collisions. Specifically, it gives a measure of the pressure anisotropy at early times.

We trust that the methods and techniques developed and used here will be useful in the evaluations of polarization signatures of real and virtual photons, evaluated with scattering kernels for momentum broadening derived from microscopic theories and using time-evolution models based in QCD.

ACKNOWLEDGMENT

C.G. acknowledges the support of the Natural Sciences and Engineering Research Council of Canada (NSERC), SAPIN-2020-00048.

APPENDIX A: THE RETARDED GLUON PROPAGATOR AT SMALL ANISOTROPY

In a system whose hard quasiparticles have the momentum distribution in Eq. (23), the retarded propagator for soft gluons is [34,36]

$$D^{\mu\nu}_{\rm ret}(Q) = \big(P_T^{\mu\nu} - C^{\mu\nu}\big)D^B_{\rm ret} + \big[(Q^2-\Pi_c)P_L^{\mu\nu} + (Q^2-\Pi_L)C^{\mu\nu} + \Pi_d D^{\mu\nu}\big]D^A_{\rm ret}, \tag{A1}$$

where

$$D^A_{\rm ret} = \frac{1}{(Q^2-\Pi_L)(Q^2-\Pi_c) - \frac{Q^2\mathbf{q}^2}{q_0^2}\Pi_d^2} \tag{A2}$$

and

$$D^B_{\rm ret} = \frac{1}{Q^2-\Pi_e}. \tag{A3}$$

The tensors $P_T^{\mu\nu}$ and $P_L^{\mu\nu}$ are the same as in thermal equilibrium while $C^{\mu\nu}$ and $D^{\mu\nu}$ are new tensors that depend on the anisotropy vector $\mathbf{n}$. The self-energy components Π_e, Π_L, Π_T, and Π_d are given in [36] which contains further details.

As $\Pi_d = \mathcal{O}(\xi)$ we can approximate

$$D^A_{\rm ret} \approx \frac{1}{(Q^2-\Pi_L)(Q^2-\Pi_c)} \tag{A4}$$

up to order $\mathcal{O}(\xi)$. We furthermore ignore $\mathcal{O}(\xi)$ corrections in the numerator as they do not describe anisotropic corrections to screening which are the nonequilibrium corrections we focus on. Then

$$\begin{aligned} D^{\mu\nu}_{\rm ret}(Q) &\approx \big(P_T^{\mu\nu} - C^{\mu\nu}\big)D^B_{\rm ret} \\ &\quad + \big[(Q^2-\Pi_c)P_L^{\mu\nu} + (Q^2-\Pi_L)C^{\mu\nu}\big]D^A_{\rm ret} \\ &= \frac{P_T^{\mu\nu}-C^{\mu\nu}}{Q^2-\Pi_e} + \frac{P_L^{\mu\nu}}{Q^2-\Pi_L} + \frac{C^{\mu\nu}}{Q^2-\Pi_c}. \end{aligned} \tag{A5}$$

The terms with the tensor $C^{\mu\nu}$ are

$$C^{\mu\nu}\left[\frac{-1}{Q^2-\Pi_e} + \frac{1}{Q^2-\Pi_c}\right] = C^{\mu\nu}\frac{\Pi_c-\Pi_e}{(Q^2-\Pi_e)(Q^2-\Pi_c)} \tag{A6}$$

which can be ignored as $\Pi_c - \Pi_e = \mathcal{O}(\xi)$ in the numerator. We are thus left with

$$D^{\mu\nu}_{\rm ret}(Q) \approx \frac{P_T^{\mu\nu}}{Q^2-\Pi_e} + \frac{P_L^{\mu\nu}}{Q^2-\Pi_L} \tag{A7}$$

at small anisotropy where we only include anisotropic corrections in the denominators. The tensors P_L and P_T are the same as in equilibrium while Π_e and Π_L have anisotropic corrections. (We call $\Pi_e = \Pi_T$ in the main text of the paper.)

APPENDIX B: DETAILS OF NUMERICAL METHOD

In this Appendix we discuss how to solve Eqs. (49) and (50) numerically. Unlike the isotropic equation, Eq. (45), the anisotropic equation has a nonvanishing source term on the right hand side for all values of b. One thus needs a different numerical solution method than that developed in [37,42,43] for the equilibrium case. We note that the differential equation for the function $f_1^{(3)}$ is

$$\mathcal{K}\big[f_1^{(3)}(\mathbf{b})\big] + \frac{ik}{2p(p+k)}\frac{8}{b^2}f_1^{(3)}(\mathbf{b}) + \mathcal{C}_0(b)f_1^{(3)}(\mathbf{b}) = -\frac{1}{2}\mathcal{C}_1^{(b)}(b)f_0 \tag{B1}$$

but we will not discuss this function further as it is not needed to evaluate A_z and A_y in Eqs. (52) and (53).

For concreteness, we focus on solving Eq. (49). Defining a scaled function

$$G = \frac{\pi}{2}\frac{k}{p(p+k)m_\infty^2}\frac{f_1^{(1z)}(b)}{b}, \tag{B2}$$

as well as scaled collision kernels $\overline{\mathcal{C}}(t) = \frac{2p(p+k)}{k}\frac{1}{m_\infty^2}\mathcal{C}(b)$ and variable $t = m_\infty b$, this equation becomes

$$-i\left[\frac{d^2G}{dt^2} + \frac{3}{t}\frac{dG}{dt} - G\right] + \overline{\mathcal{C}}_0(t)G = -\left[\overline{\mathcal{C}}_1^{(a)}(t) + \frac{1}{2}\overline{\mathcal{C}}_1^{(b)}(t)\right]\overline{f}_0(t), \tag{B3}$$

where $\overline{f}_0(t) = \frac{\pi}{2}\frac{k}{p(p+k)m_\infty^2}\mathbf{b}\cdot\mathbf{f}_0/b^2$. As shown in [37], we can write $\overline{f}_0(t) = K_1(t)/t + \overline{f}_0^{\rm rest}(t)$, where $\overline{f}_0^{\rm rest}(t)$ is function that is finite in the limit $t \to 0$ and which we know numerically using the methods of [37,42].

We need to solve Eq. (B3), imposing the boundary conditions that $G(t) \to 0$ as $t \to \infty$, as well as that $G(t)$ is finite

as $t \to 0$. These boundary conditions are difficult to satisfy simultaneously for a numerical solution. Instead we find a numerical solutions $g(t)$ of Eq. (B3) with $g(t \to \infty) = 0$ and a solution of the homogeneous equation without the source term that also satisfies $g_0(t \to \infty) = 0$. In general, both $g(t)$ and $g_0(t)$ blow up as $t \to 0$. However, we know that the solution we are seeking can be written as

$$G(t) = g(t) + Ag_0(t), \tag{B4}$$

where A is chosen so that $G(0)$ is finite.

We can find an explicit expression of A by using analytic solutions of Eq. (B3) for $t \ll 1$. In that limit the right hand side is

$$\begin{aligned}&\left[\overline{C}_1^{(a)}(t) + \tfrac{1}{2}\overline{C}_1^{(b)}(t)\right]\overline{f}_0(t)\\ &\quad\approx \left[\overline{C}_1^{(a)}(t) + \tfrac{1}{2}\overline{C}_1^{(b)}(t)\right]K_1(t)/t \approx a + b\log t,\end{aligned} \tag{B5}$$

where a and b are constants that depend on the momenta k and p as well as the masses m_D^2 and m_∞^2. The differential equation becomes

$$-i\left[\frac{d^2g}{dt^2} + \frac{3}{t}\frac{dg}{dt} - g\right] + \overline{C}_0(t)g = a + b\log t \tag{B6}$$

which has general solution

$$g(t) = w(t) + \alpha_1 w_1(t) + \alpha_2 w_2(t), \tag{B7}$$

where

$$w(t) = -ia - ib\left(\log t + \frac{2}{t^2}\right) \tag{B8}$$

is an exact particular solution and $w_2(t) = 2J_1(it)/(it)$ and $w_1(t) = \frac{\pi}{2}Y_1(-it)/(-it) - \frac{1}{4}(2\gamma_E - 2\log 2 + i\pi)w_2(t)$ are solutions of the homogenous equation such that $w_1(t) = 1/t^2 + \frac{1}{2}\log t + \mathcal{O}(1)$ and $w_2(t) = \mathcal{O}(1)$ for small t. Similarly, the homogeneous equation can be written as

$$g_0(t) = \beta_1 w_1(t) + \beta_2 w_2(t). \tag{B9}$$

The coefficients α_1, α_2, β_1, and β_2 can be found from Eqs. (B7) and (B9) by equating the numerical solutions $g(t)$ and $g_0(t)$ and their derivatives with the analytic functions at some small value $t_{\min} \ll 1$.

The small t behavior of Eqs. (B7) and (B9) shows that

$$A = \frac{2ib - \alpha_1}{\beta_1} \tag{B10}$$

which makes

$$G(0) = -ia - \frac{1}{2}ib + \alpha_2 + \frac{(2ib - \alpha_1)\beta_2}{\beta_1} \tag{B11}$$

finite. This is the expression that we need in order to evaluate Eq. (52). All quantities are known for numerical solutions $g(t)$ and $g_0(t)$.

Equation (B11) suffers from numerical cancellation errors in the terms $\alpha_2 - \alpha_1\beta_2/\beta_1$. It is thus better to rewrite these terms using Eqs. (B7) and (B9) which shows that

$$\alpha_2 - \frac{\alpha_1\beta_2}{\beta_1} = \frac{g'g_0 - gg_0' + g_0'w - g_0w'}{g_0w_2' - g_0'w_2}, \tag{B12}$$

where all quantities are evaluated at $t_{\min} \ll 1$. The culprit behind cancellation errors is the term $g'g_0 - gg_0'$. It can be evaluated more precisely by noting that

$$\mathcal{G}_W(t) = g'(t)g_0(t) - g(t)g_0'(t) \tag{B13}$$

solves the equation

$$\frac{d(t^3\mathcal{G}_W)}{dt} = -it^3\left[\overline{C}_1^{(a)}(t) + \frac{1}{2}\overline{C}_1^{(b)}(t)\right]\overline{f}_0(t)g_0 \tag{B14}$$

which can be integrated to give $\mathcal{G}_W(t_{\min})$ and thus a reliable value of $G(0)$.

[1] G. Aarts *et al.*, Phase transitions in particle physics – Results and perspectives from lattice quantum chromo-dynamics, Prog. Part. Nucl. Phys. **133** 104070 (2023).

[2] Y. Aoki, G. Endrodi, Z. Fodor, S. D. Katz, and K. K. Szabo, The order of the quantum chromodynamics transition predicted by the standard model of particle physics, Nature (London) **443**, 675 (2006).

[3] W. Busza, K. Rajagopal, and W. van der Schee, Heavy ion collisions: The big picture, and the big questions, Annu. Rev. Nucl. Part. Sci. **68**, 339 (2018).

[4] M. Strickland, Small system studies: A theory overview, Nucl. Phys. A **982**, 92 (2019).

[5] M. R. Heffernan, C. Gale, S. Jeon, and J.-F. Paquet, Bayesian quantification of strongly-interacting matter with color glass condensate initial conditions, arXiv:2302.09478.

[6] D. Everett *et al.* (JETSCAPE Collaboration), Phenomenological constraints on the transport properties of QCD matter with data-driven model averaging, Phys. Rev. Lett. **126**, 242301 (2021).

[7] D. Everett *et al.* (JETSCAPE Collaboration), Multisystem Bayesian constraints on the transport coefficients of QCD matter, Phys. Rev. C **103**, 054904 (2021).

[8] G. Nijs, W. van der Schee, U. Gürsoy, and R. Snellings, Bayesian analysis of heavy ion collisions with the heavy ion computational framework Trajectum, Phys. Rev. C **103**, 054909 (2021).

[9] J. E. Bernhard, J. S. Moreland, and S. A. Bass, Bayesian estimation of the specific shear and bulk viscosity of quark–gluon plasma, Nat. Phys. **15**, 1113 (2019).

[10] C. Gale, Photon production in hot and dense strongly interacting matter, Landolt-Bornstein **23**, 445 (2010).

[11] S. Hauksson, S. Jeon, and C. Gale, Photon emission from quark-gluon plasma out of equilibrium, Phys. Rev. C **97**, 014901 (2018).

[12] S. Hauksson, S. Jeon, and C. Gale, Probes of the quark-gluon plasma and plasma instabilities, Phys. Rev. C **103**, 064904 (2021).

[13] G. Baym and T. Hatsuda, Polarization of direct photons from gluon anisotropy in ultrarelativistic heavy ion collisions, PTEP **2015**, 031D01 (2015).

[14] B. Schenke and M. Strickland, Photon production from an anisotropic quark-gluon plasma, Phys. Rev. D **76**, 025023 (2007).

[15] L. Bhattacharya, R. Ryblewski, and M. Strickland, Photon production from a nonequilibrium quark-gluon plasma, Phys. Rev. D **93**, 065005 (2016).
[16] P. B. Arnold, G. D. Moore, and L. G. Yaffe, Photon emission from ultrarelativistic plasmas, J. High Energy Phys. 11 (2001) 057.
[17] P. B. Arnold, G. D. Moore, and L. G. Yaffe, Photon emission from quark-gluon plasma: Complete leading order results, J. High Energy Phys. 12 (2001) 009.
[18] P. B. Arnold, G. D. Moore, and L. G. Yaffe, Photon and gluon emission in relativistic plasmas, J. High Energy Phys. 06 (2002) 030.
[19] J. Ghiglieri, J. Hong, A. Kurkela, E. Lu, G. D. Moore, and D. Teaney, Next-to-leading order thermal photon production in a weakly coupled quark-gluon plasma, J. High Energy Phys. 05 (2013) 010.
[20] R. Baier, H. Nakkagawa, A. Niegawa, and K. Redlich, Production rate of hard thermal photons and screening of quark mass singularity, Z. Phys. C: Part. Fields **53**, 433 (1992).
[21] J. I. Kapusta, P. Lichard, and D. Seibert, High-energy photons from quark - gluon plasma versus hot hadronic gas, Phys. Rev. D **44**, 2774 (1991); **47**, 4171(E) (1993).
[22] H.-U. Yee, Flows and polarization of early photons with magnetic field at strong coupling, Phys. Rev. D **88**, 026001 (2013).
[23] S.-Y. Wu and D.-L. Yang, Holographic photon production with magnetic field in anisotropic plasmas, J. High Energy Phys. 08 (2013) 032.
[24] D. Ávila, T. Monroy, F. Nettel, and L. Patiño, Emission of linearly polarized photons in a strongly coupled magnetized plasma from the gauge/gravity correspondence, Phys. Lett. B **817**, 136287 (2021).
[25] L. Dong and S. Lin, Dilepton helical production in a vortical quark-gluon plasma, Eur. Phys. J. A **58**, 176 (2022).
[26] K. A. Mamo and H.-U. Yee, Spin polarized photons and dileptons from axially charged plasma, Phys. Rev. D **88**, 114029 (2013).
[27] A. Ipp, A. Di Piazza, J. Evers, and C. H. Keitel, Photon polarization as a probe for quark-gluon plasma dynamics, Phys. Lett. B **666**, 315 (2008).
[28] G. Baym, T. Hatsuda, and M. Strickland, Virtual photon polarization in ultrarelativistic heavy-ion collisions, Phys. Rev. C **95**, 044907 (2017).
[29] E. Shuryak, Monitoring parton equilibration in heavy ion collisions via dilepton polarization, arXiv:1203.1012.
[30] E. Speranza, A. Jaiswal, and B. Friman, Virtual photon polarization and dilepton anisotropy in relativistic nucleus–nucleus collisions, Phys. Lett. B **782**, 395 (2018).
[31] P. Aurenche, F. Gelis, H. Zaraket, and R. Kobes, Bremsstrahlung and photon production in thermal QCD, Phys. Rev. D **58**, 085003 (1998).
[32] M. E. Peskin and D. V. Schroeder, *An Introduction to Quantum Field Theory* (Addison-Wesley, Reading, MA, 1995).
[33] R. K. Ellis, W. J. Stirling, and B. R. Webber, *QCD and Collider Physics* (Cambridge University Press, Cambridge, 2011), Vol. 8.
[34] P. Romatschke and M. Strickland, Collective modes of an anisotropic quark-gluon plasma, Phys. Rev. D **68**, 036004 (2003).
[35] M. Martinez and M. Strickland, Dissipative dynamics of highly anisotropic systems, Nucl. Phys. A **848**, 183 (2010).
[36] S. Hauksson, S. Jeon, and C. Gale, Momentum broadening of energetic partons in an anisotropic plasma, Phys. Rev. C **105**, 014914 (2022).
[37] P. Aurenche, F. Gelis, and H. Zaraket, A Simple sum rule for the thermal gluon spectral function and applications, J. High Energy Phys. 05 (2002) 043.
[38] S. Caron-Huot, O(g) plasma effects in jet quenching, Phys. Rev. D **79**, 065039 (2009).
[39] M. Panero, K. Rummukainen, and A. Schäfer, Lattice study of the jet quenching parameter, Phys. Rev. Lett. **112**, 162001 (2014).
[40] G. D. Moore, S. Schlichting, N. Schlusser, and I. Soudi, Non-perturbative determination of collisional broadening and medium induced radiation in QCD plasmas, J. High Energy Phys. 10 (2021) 059.
[41] S. Mrowczynski, B. Schenke, and M. Strickland, Color instabilities in the quark–gluon plasma, Phys. Rep. **682**, 1 (2017).
[42] P. Aurenche, F. Gelis, G. D. Moore, and H. Zaraket, Landau-Pomeranchuk-Migdal resummation for dilepton production, J. High Energy Phys. 12 (2002) 006.
[43] S. Jeon and G. D. Moore, Energy loss of leading partons in a thermal QCD medium, Phys. Rev. C **71**, 034901 (2005).